CrossMark

ORIGINAL PAPER

# Evaluation of different nitrous oxide production models with four continuous long-term wastewater treatment process data series

Mathieu Spérandio[1,2,3] · Mathieu Pocquet[1,2,3] · Lisha Guo[4] · Bing-Jie Ni[5] ·
Peter A. Vanrolleghem[4] · Zhiguo Yuan[5]

**Abstract** Five activated sludge models describing $N_2O$ production by ammonium oxidising bacteria (AOB) were compared to four different long-term process data sets. Each model considers one of the two known $N_2O$ production pathways by AOB, namely the AOB denitrification pathway and the hydroxylamine oxidation pathway, with specific kinetic expressions. Satisfactory calibration could be obtained in most cases, but none of the models was able to describe all the $N_2O$ data obtained in the different systems with a similar parameter set. Variability of the parameters can be related to difficulties related to undescribed local concentration heterogeneities, physiological adaptation of micro-organisms, a microbial population switch, or regulation between multiple AOB pathways. This variability could be due to a dependence of the $N_2O$ production pathways on the nitrite (or free nitrous acid—FNA) concentrations and other operational conditions in different systems. This work gives an overview of the potentialities and limits of single AOB pathway models. Indicating in which condition each single pathway model is likely to explain the experimental observations, this work will also facilitate future work on models in which the two main $N_2O$ pathways active in AOB are represented together.

✉ Mathieu Spérandio
sperandio@insa-toulouse.fr

1 INSA, UPS, INP, LISBP, Université de Toulouse, 135 Avenue de Rangueil, 31077 Toulouse, France

2 INRA, UMR792 Ingénierie des Systèmes Biologiques et des Procédés, 31400 Toulouse, France

3 CNRS, UMR5504, 31400 Toulouse, France

4 modelEAU, Département de génie civil et de génie des eaux, Université Laval, Quebec, QC G1V 0A6, Canada

5 Advanced Water Management Centre, The University of Queensland, St Lucia QLD 4072, Australia

## Introduction

$N_2O$ is a powerful greenhouse gas that can be emitted from wastewater treatment plants (WWTP). The emission varies with the design and operation of a WWTP. Measurement campaigns demonstrated high temporal and spatial variability in the fraction of influent nitrogen load emitted as $N_2O$, reportedly in the range of 0.01 to more than 10 % [1, 2]. Both denitrification and nitrification processes can produce $N_2O$. However, recent measurement campaigns have conclusively shown that ammonium oxidising bacteria (AOB) in most cases contribute significantly more to $N_2O$ production than heterotrophic denitrification [3–5], whereas heterotrophic denitrification may play an important role in the removal of $N_2O$ produced by AOB [6, 7].

To evaluate the influence of process configuration and operation on the $N_2O$ emission, a significant effort has been recently devoted to $N_2O$ modelling. For dynamic modelling of $N_2O$ production, new model components have been proposed to enhance the commonly used nitrification and denitrification models at present to include various reaction intermediates such as nitrous oxide ($N_2O$), nitric oxide (NO) and hydroxylamine ($NH_2OH$).

Concerning heterotrophic denitrification, $N_2O$ and NO are known to be intermediate compounds. These compounds were included in the ASMN model proposed by Hiatt and

Springer

Grady [8] considering four successive steps in denitrification. The accumulation rate of NO and $N_2O$ depends on the relative rates of the successive steps. More recently Pan et al. [9] proposed a new model, which considers the electron competition between the different electron acceptors.

The mechanisms responsible for $N_2O$ production by AOB are more controversial. The two widely accepted mechanisms are the AOB denitrification pathway, through which AOB produce $N_2O$ via NO by reducing nitrite [10], and the hydroxylamine-related pathway. In this second mechanism, incomplete oxidation of hydroxylamine could form NO or NOH (nitroxyl radical) as intermediates for $N_2O$ production [10, 11]. Several mathematical models have been proposed based on these hypothesised pathways [12–15]. Ni et al. [14] evaluated four different models by calibrating these models with literature data obtained from batch experiments with activated sludge samples. As none of the models tested could reproduce all results, Ni et al. [14] suggested that a regulation between the two main pathways probably occurs, and called for more work to further identify the specific conditions under which each of the models would be applicable, and also to develop a generic model by integrating various pathways. Moreover, one issue related to model calibration with batch experiments is that the sludge history may impact the physiological state of the sludge. This is potentially leading to transient behaviour due to metabolic regulation, especially after a sudden change from biomass cultivation conditions to the batch condition. For this reason, it appeared essential that the models be confronted to long-term operational data measured in situ to better establish the characteristics of such generic model. Additionally, a model

combining the two main AOB pathways responsible of $N_2O$ production was recently proposed by Ni et al. [16]. It was based on a new approach which included intracellular metabolic variables and involved electrons transport for uncoupling oxidation and reduction. Before implementing this new type of multiple pathway models, it is proposed here to provide a state of the art in term of predicting $N_2O$ emissions with the current and more conventional AOB models based on a single pathway.

Therefore, the objective of this study is to evaluate different models through their calibration with several sets of continuous long-term data collected from different systems, to reveal the performance of these models under various process conditions. This work gives an overview of the potentialities and limits of using these models based on single AOB pathway to real sewage systems. This sheds light on the conditions under which each of the models are suitable, helping the practitioners to define the actual boundaries of current modelling approaches. Finally indicating in which condition each single pathway model is likely to explain the experimental observations, this work will also facilitate the development and the future calibration of a generic model by combining different pathways.

## Methods

### Experimental data

As detailed in Table 1, four different continuous biological systems were considered in this study: a University of Cape

**Table 1** Comparison of the experimental systems and operating conditions

| Process type | AS–UCT | SBR1 | AS–oxidation ditch | SBR2 |
|---|---|---|---|---|
| Country | The Netherlands | France | Australia | Australia |
| Wastewater type | Domestic | Agro-industry | Domestic | Domestic |
| COD/N (gCOD/gN) | 9 | 5 | 10 | 10 |
| SRT (day) | 10 | 15 | 10 | 19 |
| HRT (h) | 19 | 35 | 48 | 17 |
| DO aerobic (mgO$_2$/L) | 0.1–5.4 | 2–6.0 | 0.1–8.0 | 0.1-4.0 |
| Aerobic fraction (of time or volume) | 0.2–0.5 | 0.55 | <0.5[a] | 0.5 |
| Temperature during campaign (°C) | 21 ± 0.5 | 28 ± 0.5 | 25 ± 0.5 | 25 ± 0.5 |
| MLSS (g/L) | 2.5–3.5 | 5.3–6.3 | 2.9–3.7 | 4–4.5 |
| Reactor N-NH$_4^+$ (mgN/L) | 0–45 | 0–45 | 0–5 | 0–25 |
| Reactor N-NO$_2^-$ (mgN/L) | 0–0.1 | 0–50 | 0–0.5 | 0–2.5 |
| Reactor N-NO$_3^-$ (mgN/L) | 0–6.5 | 0–10 | 0–1 | 0–5 |
| Nitrogen load (kgN/m$^3$/day) | 0.070 | 0.267 | 0.045 | 0.074 |
| N$_2$O emission factor (gN-N$_2$O/gTN) | 0.12 % | 1.0 % | 0.36 % | 1.0 % |
| | 3.10 % | 5 % | 0.68 % | 1.5 % |
| Measurement campaign (month) | 1 | 6 | 1 | 1 |

[a] Not precisely determined

Town (UCT) process, an oxidation ditch and two sequencing batch reactors (SBR). Technical details on each system and measurement campaigns can be found in dedicated articles and communications [15, 17, 18] and supplementary information (Table S1).

The SBR1 is a lab-scale pilot which was operated for more than 6 months. It was fed with a nitrogen rich wastewater (500 mgN-NH$_4^+$ L$^{-1}$). Cycles consisted of five phases, i.e. feeding, aerobic reaction, anoxic reaction, settling and withdrawal. A complement in organic carbon for denitrification was provided by a lactose-rich solution (whey). An average volumetric loading rate of 2.79 kgCOD m$^{-3}$ day$^{-1}$ was obtained. This carbon source was provided for a short period at the beginning of the anoxic period to maintain a suitable COD:N ratio (from 3.5 to 5). Various volumetric exchange ratios were imposed to adapt the ammonium concentration in the reactor. The system was operated in view of shortcut nitrogen removal over nitrite by controlling the duration of aeration. This strategy consists of stopping aeration as soon as ammonia is depleted which limits the oxidation of nitrite to nitrate. The process was operated at a high ammonia loading rate (0.267 kg N m$^{-3}$ day$^{-1}$) and exhibited nitrite accumulation during aerobic periods. The average hydraulic retention time (HRT) is 35 h. The solids retention time (SRT) is 15 day.

The full-scale oxidation ditch (OD) plant receives domestic wastewater at approximately 4000 m$^3$ per day (approx. 20,000 population equivalent noted PE). The plant consists of a primary clarifier and an activated sludge system with surface aerators. After primary sedimentation, wastewater is introduced into the activated sludge unit with a working volume of 8750 m$^3$. The average hydraulic retention time (HRT) in the OD is 34 h. The solids retention time (SRT) is approximately 12 day. More details about data collection are given by Ni et al. [15].

Data collected from a full-scale SBR plant (SBR2) are also considered. The average daily flow of the plant is 120,000 m$^3$ per day (approx. 600,000 PE). The plant consists of a primary sedimentation tank followed by secondary treatment. The biological nutrient removal component of the plant comprises a circular tank that is evenly quartered into four basins. Each basin operates as a separate SBR. At the time of this study, each SBR cycle consisted of the following phases in sequence: 90 min continuous feeding and aeration, 35 min settling and 55 min decanting. The average exchange volume per cycle in each SBR was approximately 5000 m$^3$. Each SBR had a working volume of 28,000 m$^3$, and hence the average HRT was 17 h. The total airflow to the three SBRs was fixed at 45,000 m$^3$ h$^{-1}$ throughout the aeration phase with equal distribution among the three reactors. The SRT was maintained at 19 days.

The Eindhoven WWTP, in the Netherlands, has a capacity of 750,000 PE. It treats wastewater using a University Cape Town (UCT) process, implemented with three rings. The inner ring is an anaerobic tank, the middle ring is an anoxic tank and the outer ring is a partially aerated tank. The outer ring is equipped with two aeration zones. The so-called summer aeration zone functions all year round, but the winter aeration zone is only turned on in winter conditions and occasionally under certain conditions, e.g. under rain events. The SRT was 10 days and the overall hydraulic retention time was 19 h. More details can be found in Guo and Vanrolleghem [17].

Long-term and/or intensive measurement campaigns for quantification of N$_2$O were performed on each system (Table S1). The detailed procedures used on each plant can also be found in associated publications [15, 17, 18] with several key technical aspects underlined in this work. A special effort was dedicated to the development of an accurate quantification of N$_2$O emissions in oxidation ditch [15], particularly for the emissions from the surface aerator zone which cannot be easily captured by floating hoods. Because liquid is recirculating in a plug flow regime in the oxidation ditch, dissolved N$_2$O was measured in liquid samples using gas chromatography (GC) at different times and in different zones. It was thus possible to clearly differentiate the emissions in anoxic and aerobic zone considering both liquid accumulation and gas emissions.

The N$_2$O concentration in the off-gas was monitored using online continuous infrared (IR) spectroscopy for three of these systems (UCT and the two SBRs). Floating hood methods were used for measuring N$_2$O in the gas phase for full-scale UCT and SBR2. The N$_2$O was measured at different surface locations with a specific protocol [17]. Sampling of the off-gas was used for the lab-scale SBR1 (covered reactor). In addition, the NO concentration in the off-gas was also measured in SBR1 using an IR analyser.

In these systems, the daily average N$_2$O emission factors were quantified in gN-N$_2$O/gTN removed (Table 1). It varied from 0.12 to 3.1 % for the UCT, 1 to 5 % for the SBR1, 0.36 to 0.68 % for the OD, 1 to 1.5 % for the SBR2. The highest emission was obtained with the SBR1 working at the highest loading rate (0.267 kgN m$^{-3}$ day$^{-1}$) with the highest nitrite variation (0–50 mgN L$^{-1}$).

## Mathematical models

In this study mathematical models, all based on the ASMN framework [8], were used with additions for considering production of NO and N$_2$O by AOB. As nitrification was supposed to be the main producer of N$_2$O and because of the different possible pathways involved, different AOB models were compared. The reaction stoichiometry and kinetics of the five N$_2$O models related to AOB are summarised in Table 2.

**Table 2** Processes stoichiometry and kinetics of the five tested models for AOB

| Process | Model components | | | | | | | Kinetic rate expressions |
|---|---|---|---|---|---|---|---|---|
| | $S_{O_2}$ | $S_{NH}$ | $S_{NH_2OH}$ | $S_{NO_2}$ | $S_{NO}$ | $S_{N_2O}$ | $X_{AOB}$ | |
| **Model A—Ni et al. [13]** | | | | | | | | |
| 1 | $-\frac{8}{7}$ | $-1$ | $1$ | | | | | $\mu_{AOB,AMO} \times \frac{S_{O_2}}{K_{O_2,AOB,1}+S_{O_2}} \times \frac{S_{NH_4}}{K_{NH_4,AOB}+S_{NH_4}} \times X_{AOB}$ |
| 2 | $\frac{16/7-Y_{AOB}}{Y_{AOB}}$ | $-i_{N,AOB}$ | $-\frac{1}{Y_{AOB}}$ | $\frac{1}{Y_{AOB}}$ | | | $1$ | $\mu_{AOB,HAO} \times \frac{S_{O_2}}{K_{O_2,AOB,2}+S_{O_2}} \times \frac{S_{NH_2OH}}{K_{NH_2OH,AOB}+S_{NH_2OH}} \times X_{AOB}$ |
| 3 | | | $-1$ | $-3$ | $4$ | | | $\eta_{AOB} \times \mu_{AOB,HAO} \times \frac{K_{I,O_2,AOB}}{K_{I,O_2,AOB}+S_{O_2}} \times \frac{S_{NH_2OH}}{K_{NH_2OH,AOB}+S_{NH_2OH}} \times \frac{S_{NO_2}}{K_{NO_2,AOB}+S_{NO_2}} \times X_{AOB}$ |
| 4 | | | $-1$ | $1$ | $-4$ | $4$ | | $\eta_{AOB} \times \mu_{AOB,HAO} \times \frac{K_{I,O_2,AOB}}{K_{I,O_2,AOB}+S_{O_2}} \times \frac{S_{NH_2OH}}{K_{NH_2OH,AOB}+S_{NH_2OH}} \times \frac{S_{NO}}{K_{NO,AOB}+S_{NO}} \times X_{AOB}$ |
| **Model A1—Pocquet et al. [18]** | | | | | | | | |
| 1 | | | | | | | | $\mu_{AOB,AMO} \times \frac{S_{O_2}}{K_{O_2,AOB,1}+S_{O_2}} \times \frac{S_{NH_3}}{K_{NH_3,AOB}+S_{NH_3}+S_{NH_3}^2/K_{I,NH_3,AOB}} \times X_{AOB}$ |
| 2 | | | | | | | | $\mu_{AOB,HAO} \times \frac{S_{O_2}}{K_{O_2,AOB,2}+S_{O_2}} \times \frac{S_{NH_2OH}}{K_{NH_2OH,AOB}+S_{NH_2OH}} \times X_{AOB}$ |
| 3 | | | | | | | | $\eta_{AOB} \times \mu_{AOB,HAO} \times \frac{S_{NH_2OH}}{K_{NH_2OH,AOB}+S_{NH_2OH}} \times \frac{S_{HNO_2}}{K_{HNO_2,AOB}+S_{HNO_2}} \times X_{AOB}$ |
| 4 | | | | | | | | $\eta_{AOB} \times \mu_{AOB,HAO} \times \frac{S_{NH_2OH}}{K_{NH_2OH,AOB}+S_{NH_2OH}} \times \frac{S_{NO}}{K_{NO,AOB}+S_{NO}} \times X_{AOB}$ |
| **Model B—Mampaey et al. [12]** | | | | | | | | |
| 1 | $\frac{24/7-Y_{AOB}}{Y_{AOB}}$ | $-\frac{1}{Y_{AOB}} - i_{N,AOB}$ | | $\frac{1}{Y_{AOB}}$ | | | $1$ | $\mu_{AOB} \times \frac{S_{O_2}}{K_{O_2,AOB}+S_{O_2}} \times \frac{S_{NH_3}}{K_{NH_3,AOB}+S_{NH_3}} \times X_{AOB}$ |
| 2 | $-\frac{16/7-Y_{AOB,den}}{Y_{AOB,den}}$ | $\frac{1}{Y_{AOB,den}} - i_{N,AOB}$ | | $-\frac{1}{Y_{AOB,den}}$ | $\frac{2}{Y_{AOB,den}}$ | | $1$ | $\eta_{AOB} \times \mu_{AOB} \times \frac{S_{O_2}}{K_{O_2,AOB}+S_{O_2}} \times \frac{S_{NH_3}}{K_{NH_3,AOB}+S_{NH_3}} \times \frac{S_{HNO_2}}{K_{HNO_2,AOB}+S_{HNO_2}} \times X_{AOB}$ |
| 3 | $\frac{16/7-Y_{AOB,den}}{Y_{AOB,den}}$ | $\frac{1}{Y_{AOB,den}} - i_{N,AOB}$ | | $\frac{1}{Y_{AOB,den}}$ | $-\frac{2}{Y_{AOB,den}}$ | $\frac{2}{Y_{AOB,den}}$ | $1$ | $\eta_{AOB} \times \mu_{AOB} \times \frac{S_{O_2}}{K_{O_2,AOB}+S_{O_2}} \times \frac{S_{NH_3}}{K_{NH_3,AOB}+S_{NH_3}} \times \frac{S_{NO}}{K_{NO,AOB}+S_{NO}} \times X_{AOB}$ |
| **Model B1—Guo et al. [4]** | | | | | | | | |
| 1 | | | | | | | $1$ | $\mu_{AOB} \times \frac{S_{O_2}}{K_{O_2,AOB}+S_{O_2}} \times \frac{S_{NH_3}}{K_{NH_3,AOB}+S_{NH_3}+S_{NH_3}^2/K_{I,NH_3,AOB}} \times X_{AOB}$ |
| 2 | | | | | | | $1$ | $\eta_{AOB} \times \mu_{AOB} \times \frac{S_{NH_3}}{K_{NH_3,AOB,den}+S_{NH_3}+} \times \frac{S_{HNO_2}}{K_{HNO_2,AOB}+S_{HNO_2}} \times \frac{K_{I,HNO_2,AOB}}{K_{I,HNO_2,AOB}+S_{HNO_2}} \times X_{AOB} \times DO_{Haldane}$ |
| 3 | | | | | | | | $\eta_{AOB} \times \mu_{AOB} \times \frac{S_{NH_3}}{K_{NH_3,AOB,den}+S_{NH_3}+} \times \frac{S_{NO}}{K_{NO,AOB}+S_{NO}} \times X_{AOB} \times DO_{Haldane}$ |
| | | | | | | | | $DO_{Haldane} = \frac{S_{O_2}}{K_{O_2,AOB,den}+\left(1-2\times\sqrt{K_{O_2,AOB,den}/K_{I,O_2,AOB}}\right)S_{O_2}+S_{O_2}^2/K_{I,O_2,AOB}}$ |
| **Model C—Ni et al. [15]** | | | | | | | | |
| 1 | $-\frac{8}{7}$ | $-1$ | $1$ | | | | | $\mu_{AOB,AMO} \times \frac{S_{O_2}}{K_{O_2,AOB,1}+S_{O_2}} \times \frac{S_{NH_4}}{K_{NH_4,AOB}+S_{NH_4}} \times X_{AOB}$ |
| 2 | $\frac{12/7-Y_{AOB}}{Y_{AOB}}$ | $-i_{N,AOB}$ | $-\frac{1}{Y_{AOB}}$ | | $\frac{1}{Y_{AOB}}$ | | $1$ | $\mu_{AOB,HAO,1} \times \frac{S_{O_2}}{K_{O_2,AOB,2}+S_{O_2}} \times \frac{S_{NH_2OH}}{K_{NH_2OH,AOB}+S_{NH_2OH}} \times X_{AOB}$ |
| 3 | $-\frac{4}{7}$ | | $1$ | $1$ | $-1$ | | | $\mu_{AOB,HAO,2} \times \frac{S_{O_2}}{K_{O_2,AOB,2}+S_{O_2}} \times \frac{S_{NO}}{K_{NO,AOB}+S_{NO}} \times X_{AOB}$ |
| 4 | | | $-1$ | $1$ | $-4$ | $4$ | | $\eta_{AOB} \times \mu_{AOB,HAO,1} \times \frac{S_{NH_2OH}}{K_{NH_2OH,AOB}+S_{NH_2OH}} \times \frac{S_{NO}}{K_{NO,AOB}+S_{NO}} \times X_{AOB}$ |

Two models were based on the AOB denitrification pathway namely: the Ni et al. [13] model which does include $NH_2OH$ as an intermediate in ammonium oxidation (Model A) and the Mampaey et al. [12] model, which does not (Model B). Another key difference between these two models is the influence of oxygen: Model A only includes DO inhibition of $N_2O$ production whereas oxygen is only a limiting substrate in Model B. The third model was based on the hydroxylamine oxidation pathway (Model C). In this model, NO is considered as an intermediary compound during the oxidation of $NH_2OH$ to nitrite [13–15]. $N_2O$ is then produced by reduction of NO with the same reaction as in Model A. Note that Model C contains a modification compared to the initial model [13–15], originally growth was considered to occur in two processes, but here biomass production was removed from process 3 to use the conventional value for the growth yield ($Y_{AOB}$). Consequently the value of the new maximal rate $\mu_{AOB,HAO,2}$ is here calculated as $\mu_{AOB,HAO,1}/Y_{AOB}$.

Two modifications of the original AOB denitrification models (A, B) have also been considered [17, 18] (Models A1, B1). In Model A1, the oxygen inhibition of the AOB reduction pathway was not considered. In addition, free ammonia (FA) and free nitrous acid (FNA) were considered as the substrate for the AOB reactions, to explicitly consider the effect of pH variation. In Model B1, oxygen limitation and inhibition were considered through a Haldane function in both the kinetics of $NO_2^-$ reduction and NO reduction [6, 17]. Inhibition by FA was also considered in Model A1 and both inhibition by FA and FNA were included in Model B1.

The gas liquid transfers of oxygen, NO and $N_2O$ were also included. The transfer coefficients ($K_La$) for both NO and $N_2O$ were calculated with the measured oxygen transfer coefficient and respective diffusivity ratio [19]. In addition, the phosphorus removal and the influence of temperature were also considered for UCT process modelling including phosphorus accumulating organisms with the ASM2d framework [17]. Simulations were performed using AQUASIM [20] and WEST [21].

**Parameter calibration**

Simulation methodologies for each system were similar to well-accepted protocols for dynamic activated sludge models calibration with long-term data and were detailed elsewhere [15, 17, 18]. Physical and hydrodynamic characteristics were also considered for modelling the full-scale oxidation ditch and UCT process with appropriate combination of in series reactors [6, 15]. Wastewater characteristics were collected and solid mass balance were checked. Wastewater characteristics and COD fractionation are given in Table S1 (SI) with some key information on

hydraulic description. Oxygen transfer rate was assessed in each reactor or zone. Variables initialisation was obtained from steady state simulations related to average mass balances. The steady state biomass concentrations are given in Table S3 (SI). Simulated MLVSS were in agreement with experimental data without adaptation of the central model parameters: default values for heterotrophs decay rate and growth yield were used (ASMN: $Y_{OHO} = 0.6$ gCOD/gCOD, $b_{OHO} = 0.41$ day$^{-1}$). Parameter calibration was then performed in two steps, first considering the major rates and components (ammonia, nitrate, nitrite) and then the $N_2O$ and NO data. All the parameters of the models are given in Tables S4, S5 and S6 (SI). Whenever possible, our approach has been to use typical parameter values reported in literature [8] for most of heterotrophic and autotrophic processes (for instance, yields, decay rates and hydrolysis rates). Concerning NOB-related parameters, the prediction of nitrite concentration is very important for $N_2O$ models and must be predicted with accuracy. For example, in the case of UCT process the NOB parameters had to be adapted to predict more accurately the nitrite level in the system. Parameter estimation was basically realised manually and in a second time for a limited number of parameters, mathematical minimisation of the root mean squared error was tested for better adjustment (Newton–Raphson method). For the different systems, the data and the simulation indicated that denitrification process was not responsible of $N_2O$ emissions and can even consume $N_2O$. This is related to the presence of sufficient readily biodegradable COD for denitrification. The affinity constant dedicated to reduction of each electron acceptor ($NO_3$, $NO_2$, NO, $N_2O$) was slightly adapted for process SBR1 and UCT to match with that observation (no emission in anoxic periods).

Sensitivity analysis was performed to identify the most influential parameters on $N_2O$ and NO emissions. As an example, the results of the sensitivity analysis on $N_2O$ and NO for parameters involved in the AOB models are illustrated in supplementary information (Table S2) for the case of the SBR1. Basically for all the models and for all the systems studied, the most influential parameter related to $N_2O$ processes was the reduction factor ($\eta_{AOB}$) which impacts both the emission rate and the emission factor. Moreover, the emission rate was indirectly sensitive to core parameters which influence the nitritation rate ($Y_{AOB}$, $\mu_{AOB}$, $K_{NH4,AOB}$) but these parameters did not influence the $N_2O$ emission factor. Depending on the feeding regime (batch or continuous) the prediction of $N_2O$ responses and emission factors is more or less influenced by the affinity constant ($K_{NH2OH}$, $K_{NO2}$, $K_{NO}$). Identifiability of $\eta_{AOB}$ and $K_{HNO2}$ has been evaluated by Pocquet et al. [18] for models based on AOB denitrification. These parameters were estimated independently as soon as the explored range of

nitrite concentration was sufficiently large (situation of SBR1 for instance).

Parameters influencing ammonium, nitrite, nitrate (and indirectly NO and N$_2$O) were calibrated during the first step (e.g. $\mu_{AOB,AMO}$, $\mu_{AOB}$, $K_{NH4,AOB}$). Second, the parameters influencing only the N$_2$O emission and NO emission (with very low impact on ammonia, nitrite or nitrate) were adapted, in this way maintaining the model fit to the ammonium, nitrate and nitrite data. In this second phase, the reduction factor $\eta_{AOB}$ as well as the affinity constant $K_{NO2,AOB}$ were focused upon due to their significant influence. The NO emission is also very sensitive to the parameter $K_{NO,AOB}$ which was estimated with the NO measurements performed on SBR1.

## Results

### SBR1

All five models were examined with the data collected from SBR1. In this system more than 97 % of the ammonia was converted to nitrite during the aerobic period and only a very low level of nitrate was detected. For the five models, Fig. 1 shows examples of simulated and experimental data (NH$_4^+$, NO$_2^-$, DO, NO and N$_2$O) during the aerobic periods obtained after calibration. Depending on the cycle oxygen varied from 2 to 6 mg O$_2$ L$^{-1}$, initial ammonium from 10 to 40 mgN L$^{-1}$, and final nitrite ranged from 30 to 135 mg N L$^{-1}$. N$_2$O and NO peaks were only observed during the aerobic period whereas no emission was observed during the anoxic phase (even with nitrogen gas injection). The five models were calibrated on a series of data (five cycles) and model predictions were also validated with other cycles collected at different times in different conditions.

For all models the predicted profiles of ammonium, nitrite and DO match the observed experimental trends. The four models based on nitrite denitrification (Models A, A1, B, B1) also describe the observed N$_2$O peak well. In contrast, Model C could not predict the variation of N$_2$O peaks for the different cycles, with high discrepancies at high nitrite concentrations. In those conditions with relatively high DO, simulations indicate that N$_2$O was mainly related to AOB processes with an insignificant contribution by heterotrophic denitrification.

The order of magnitude of NO peaks was reasonably predicted by the four models based on AOB denitrification but the increase of NO with HNO$_2$ was over estimated. In comparison, model C could not predict this order of magnitude. Based on simultaneous monitoring of N$_2$O and NO, calibration of the $K_{NO}$ value was possible. However, despite significant calibration effort model C was unable to

**◀ Fig. 1** Dynamic of nitrification and NO and N$_2$O production for five experiments obtained with the SBR. Experimental results (*in points*) are confronted to modelling results (*in line*) for the five models. The dynamic of NO (*open diamond*) (secondary axis) and N$_2$O (*open circle*) (primary axis) production are presented in the first line of each models whereas ammonium (*open triangle*), nitrite (*open circle*) (primary axis) and dissolved oxygen (*open circle*) (secondary axis) are presented in the second line. Duration of experiment 1–5: 1, 0.4, 0.4, 1 and 0.4 h. Experimental N$_2$O emission factor for experiment 1–5 (in gN-N$_2$O/gN-NH$_4^+$ removed): 1.39, 2.58, 3.86, 1.83 and 4.52 %

predict the experimentally observed change in the NO to N$_2$O ratio (Table 3). Overall, the best predictions for NO and N$_2$O were observed with models A, A1, B and B1, basically because they are based on the AOB denitrification concept. Corrections made on the oxygen effect (inhibition) could also impact the simulation, but in the data used, the DO was relatively high and the constant for oxygen inhibition was thus not identifiable. It should be pointed out that this system exhibits high transient nitrite accumulation and the data indicates a correlation between nitrite and the N$_2$O production rate (Fig. 1). It was possible to predict this phenomenon with AOB denitrification models but not with the concept of incomplete hydroxylamine oxidation which is not related to nitrite (Model C).

Figure 2 compares the predicted and experimental emission factors (EF) for N$_2$O and NO for 11 different cycles (including new data used for validation). These results confirm that Models A1, B and B1 show the best prediction of N$_2$O and NO emissions, Model A also being relatively good. The predictions of NO fluctuations are less accurate than for N$_2$O but the ratio between both gases is relatively well predicted by the models that use the AOB denitrification pathway (Table 3). Model C based on the NH$_2$OH/NO pathway could not predict the experimental data as it is unable to predict the effect of nitrite accumulation on N$_2$O and NO production. This leads to an underestimation of N$_2$O emission at high FNA concentrations whereas NO emission is overestimated.

### Oxidation ditch

The original AOB denitrification models (Models A, B) and the NH$_2$OH/NO model (Model C) were examined with the experimentally observed continuous N$_2$O data from the full-scale oxidation ditch (OD). The models were calibrated using the extensive monitoring data from a 3-day intensive sampling campaign at three different locations (OD4-aeration zone, OD5-aerobic zone near the propulsor and OD2-anoxic zone) of the ditch. Figure 3 shows the simulated and experimental data (NH$_4^+$, NO$_2^-$, NO$_3^-$ and N$_2$O) at the three locations along the ditch. The N$_2$O emissions
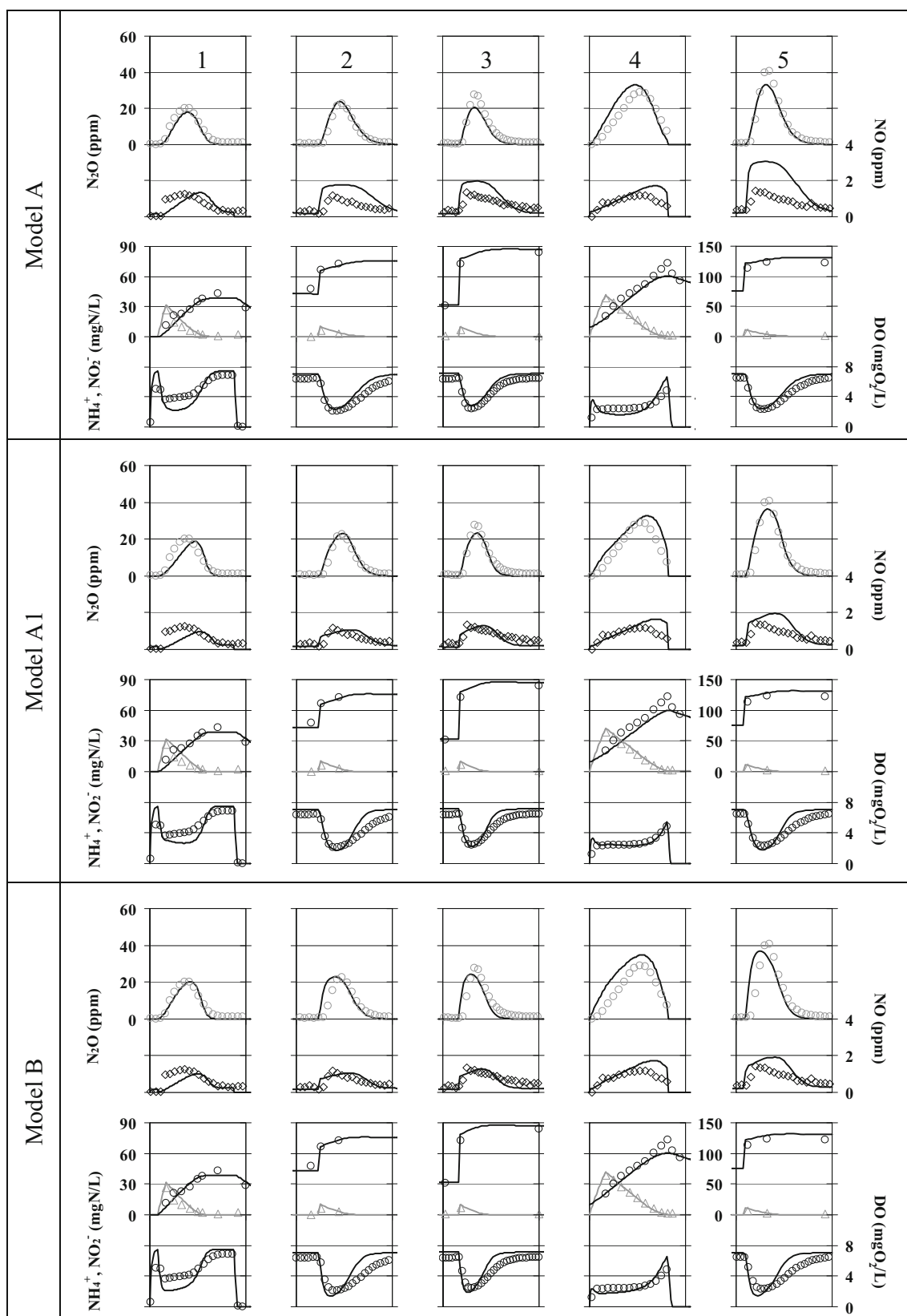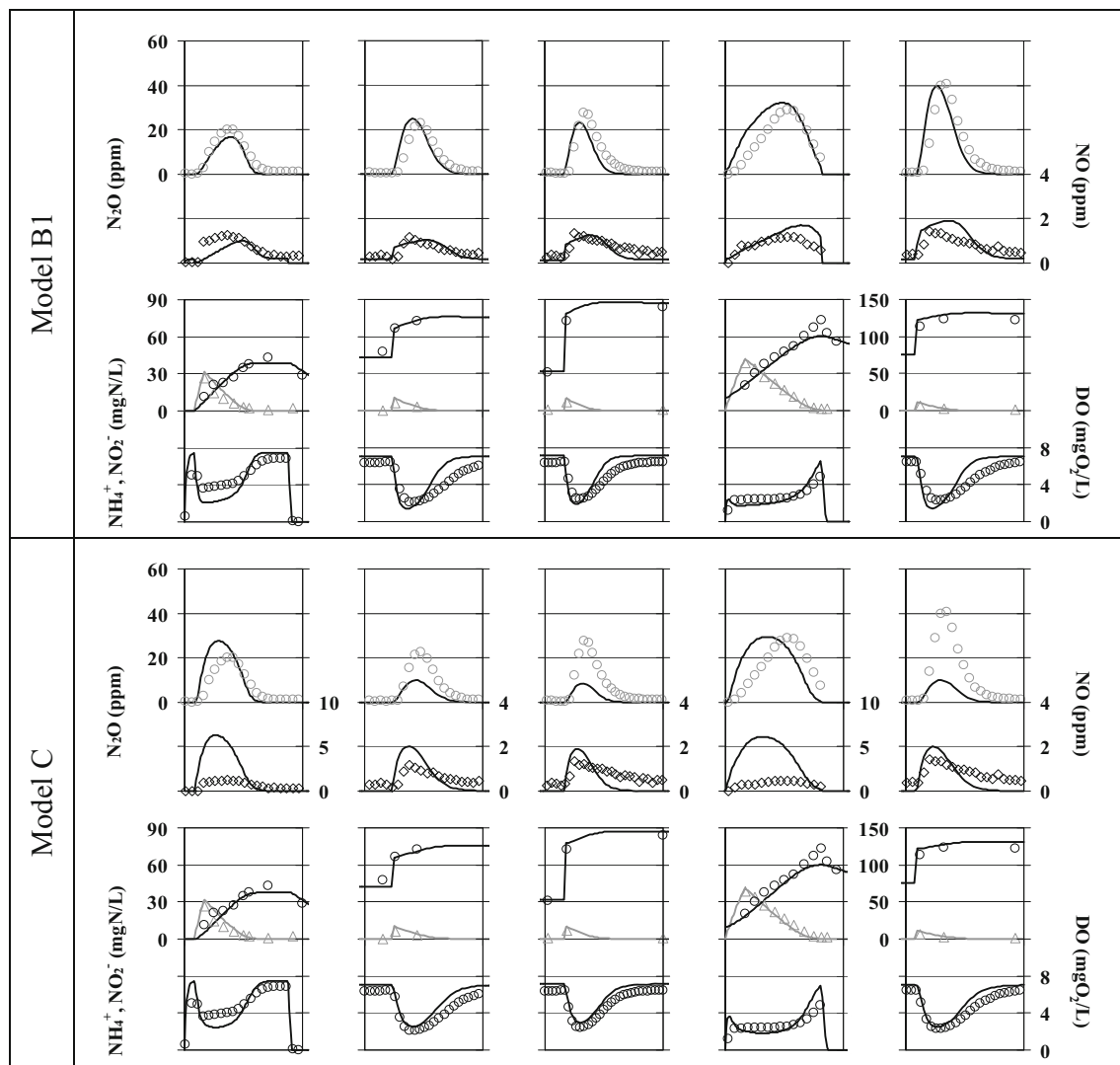
**Fig. 1** continued

occurred mainly in aerobic zones (OD4) with high ammonium concentrations but low nitrite accumulation.

For the three models (A, B, C) the predicted profiles of ammonium, nitrite and nitrate match the observed experimental trends. However, the results indicate that Model A cannot predict the N₂O data. Indeed, Model A predicts a dependency of N₂O production on DO that is opposite to that observed at the OD plant (Fig. 3a–f). Conversely, the kinetic structure of Model B ensures that the N₂O production rate is dependent on oxygen availability, resulting in a N₂O dynamic trend similar to that shown by the experimental data (Fig. 3g–l). However, for Model B to reasonably predict the N₂O production rate when nitrite accumulation in the OD system is very low (<0.67 mgN/L), a relatively high anoxic reduction factor (0.63) has to be employed due to the fact that the N₂O production rate is dependent on nitrite concentrations (this point is discussed

below). In contrast, Model C achieves a good fit between the model-predicted and measured N₂O data. The NH₂OH pathway of Model C captures all observed trends.

## SBR2

The original Models A, B and C were also evaluated with the experimentally observed N₂O data from a full-scale SBR plant (SBR2). The models were calibrated using the monitoring data collected from SBR2 during a three-cycle continuous intensive sampling campaign. Figure 4 shows the simulated and experimental data (effluent NH₄⁺, NO₂⁻, NO₃⁻ and N₂O) during the three-cycles. Similar to the OD system, SBR2 also has low nitrite accumulation. In SBR2, N₂O emissions occurred mainly during aerated periods. The N₂O production rate increased with the increase of DO concentration during the SBR2 cycles.

**Table 3** Comparison between experimental and simulated NO to $N_2O$ ratio from SBR1

| Experiment/cycle | NO/$N_2O$ ratio (gN-NO/gN-$N_2O$) in percentage (%) | | | | |
|---|---|---|---|---|---|
| | 1 | 2 | 3 | 4 | 5 |
| Data | 4.4 | 4.6 | 4.9 | 2.9 | 3.5 |
| Model A | 5.3 | 7.5 | 9.2 | 2.9 | 8.6 |
| Model A1 | 3.6 | 4.2 | 4.9 | 2.5 | 4.6 |
| Model B | 3.5 | 4.2 | 4.7 | 2.4 | 2.4 |
| Model B1 | 4.1 | 4.2 | 5.2 | 2.7 | 4.5 |
| Model C | 12.0 | 10.7 | 11.6 | 10.5 | 10.8 |

Again, for the three models the predicted profiles of ammonium, nitrite and nitrate match the observed experimental trends. As before, Model A predicts an $N_2O$ trend opposite to that observed, while Models B and C achieve a good fit between the model-predicted and measured $N_2O$ data. For Model B again, based on nitrite reduction pathway, a high reduction factor $\eta_{AOB}$ (0.56) has to be used as the $N_2O$ production rate is related to nitrite concentrations which was low in the SBR2.

## UCT process

Dynamic simulations were confronted to the data collected on the UCT process from the Eindhoven plant. Model A1, Model B1 and Model C were implemented for this plant and their parameters were calibrated using data collected in a 1-month measurement campaign. Figure 5 compares the simulated $NH_4^+$, $NO_3^-$ and DO concentrations with the online sensor data near the outlet of the summer aeration zone. Figure 6 compares the simulation and the
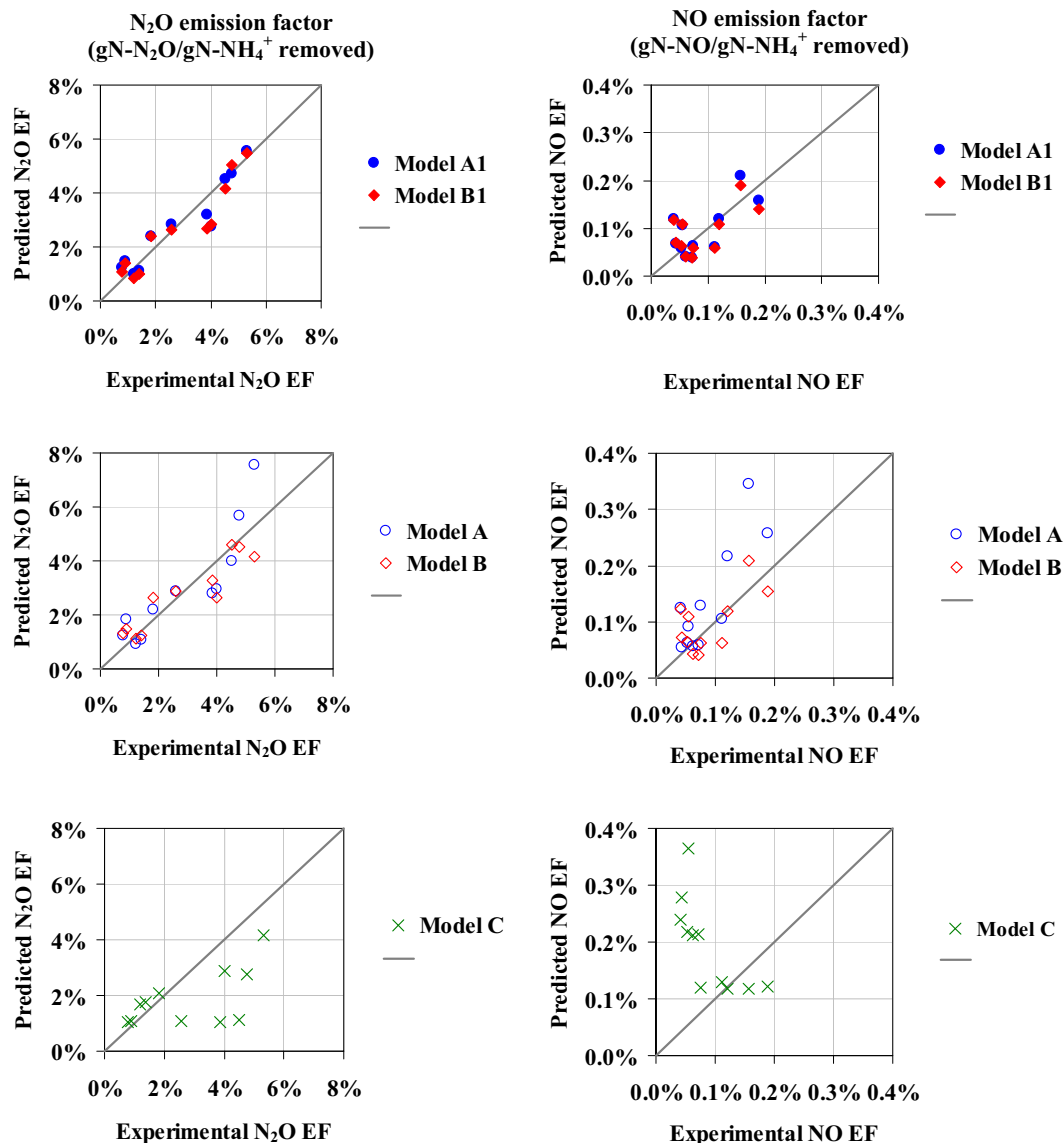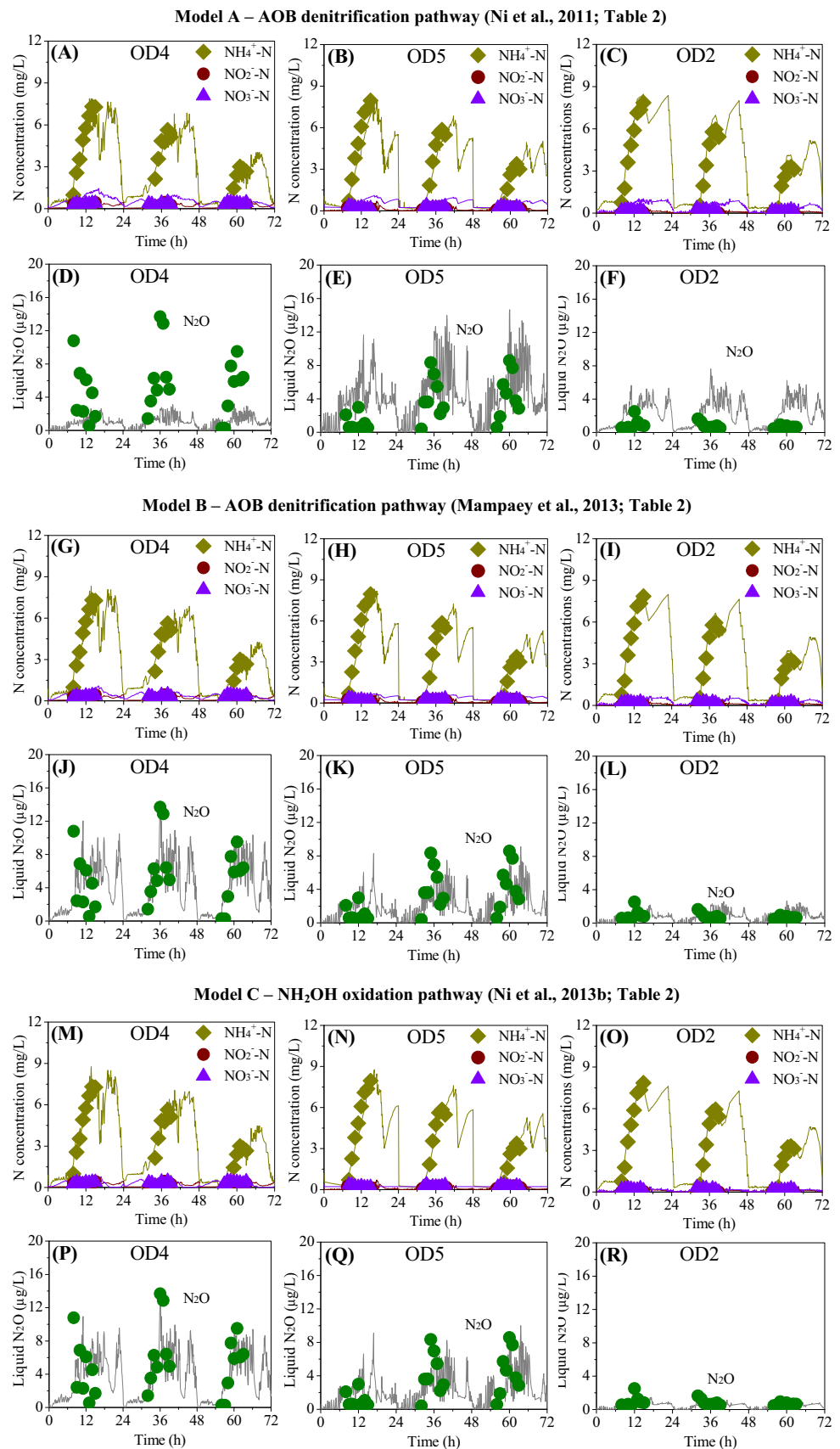


**Fig. 2** Comparison between experimental and predicted $N_2O$ and NO emission factors for different cycles (11) obtained with the SBR1

**Fig. 3** Model evaluation results of the three-day N₂O production data from the Oxidation Ditch WWTP (experimental data: *symbols*; model predictions: *lines*) with ammonium, nitrite, nitrate and liquid phase N₂O profiles at the different sampling locations (OD4, OD5 and OD2): **a–f** Model A; **g–l** Model B and **m–r** Model C
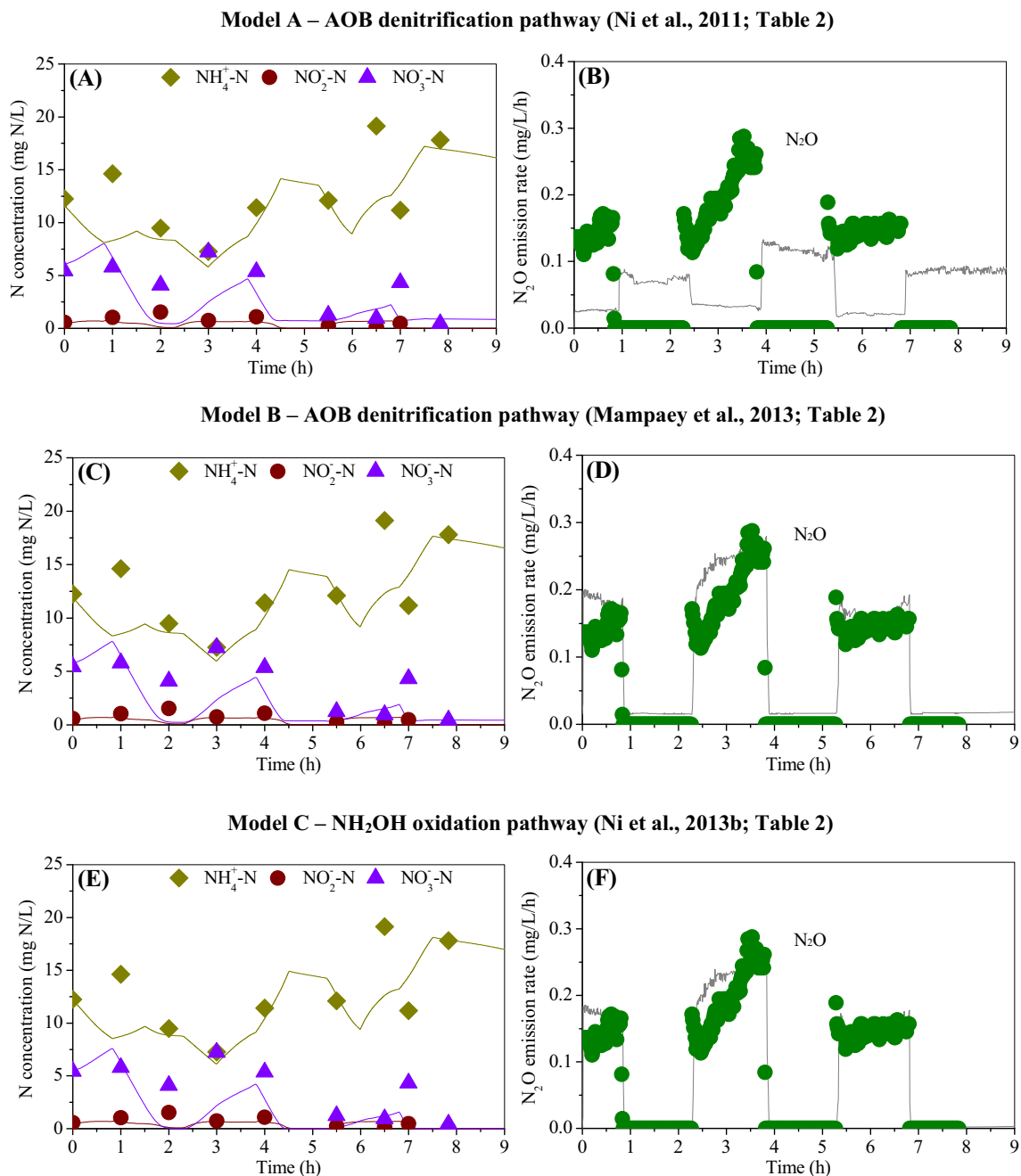
**Model A – AOB denitrification pathway (Ni et al., 2011; Table 2)**



**Model B – AOB denitrification pathway (Mampaey et al., 2013; Table 2)**



**Model C – NH₂OH oxidation pathway (Ni et al., 2013b; Table 2)**



**Fig. 4** Model evaluation results of the $N_2O$ production data from SBR (2) WWTP (experimental data: *symbols*; model predictions: *lines*) with ammonium, nitrite, nitrate and $N_2O$ emission rate profiles: **a–b** Model A; **c–d** Model B and **e–f** Model C

measurement data of $N_2O$ emissions at three different locations along the summer aeration zone. The conclusion is that all models can be calibrated to the same level of fit. They have similar performance and can follow the dynamic variations in the measurement data. There was a rain event on August 25th–26th. All models showed better simulation performance under dry-weather conditions than wet-weather conditions (Fig. 5). Results show that there was less $N_2O$ emission under wet-weather conditions compared to dry-weather conditions (Fig. 6).

## Discussion

### Observed $N_2O$ emissions and capabilities of the models

The data monitored on the four continuous systems considered in this study confirm that the $N_2O$ emission factors varied very significantly from 0.1 to 5.2 % of the nitrogen removed. Data and simulations also confirmed that nitrification is the major contributor to $N_2O$ production. For
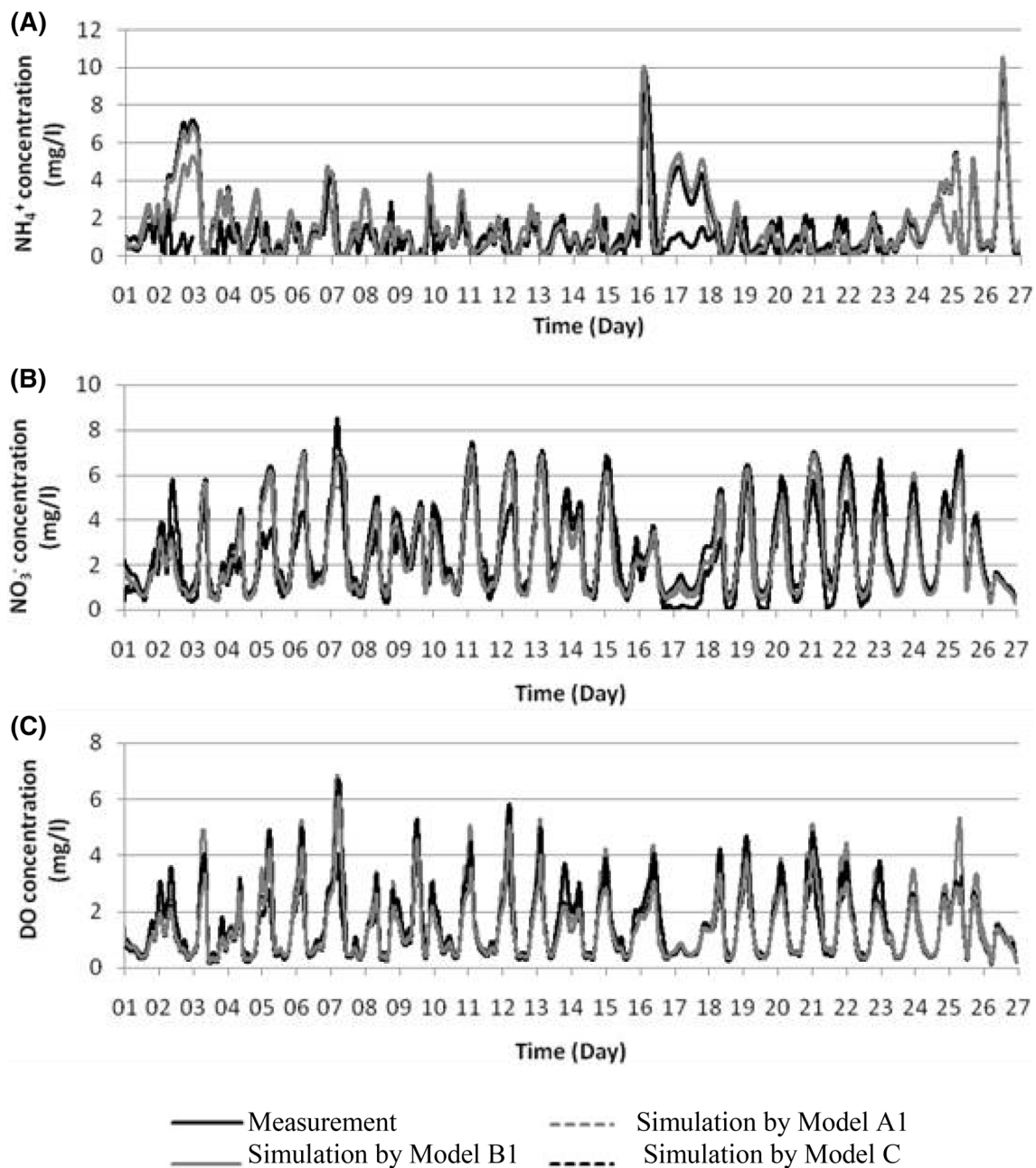
**(A)**



**(B)**

**(C)**

Fig. 5 Comparison of the measurement results with the simulation results of NH4+ (**a**), NO3− (**b**) and DO (**c**) near the outlet of the summer aeration package at the UCT plant

instance, N$_2$O emissions were negligible in SBR1 during anoxic periods (checked with punctual nitrogen insufflations) probably thanks to a sufficient COD:N ratio for complete denitrification. In contrast, 0.5–5 % of nitrogen was converted to N$_2$O during aerobic nitrification depending on the FNA concentration (DO from 2 to 6 mg L$^{-1}$). In OD the overall N$_2$O emission factor over a full month was 0.52 % of the nitrogen load to the plant, with over 90 % contribution from the aeration zone (DO of over 5 mg L$^{-1}$). These data were issued from both liquid

mass balance and gas emissions. Similarly, the N$_2$O emission factor of the SBR2 over the month is around 1.0–1.5 % of the nitrogen load, with N$_2$O emissions occurring mainly during aerated periods. Simulation of the UCT process (with Model B1) was used for quantifying the average contribution of heterotrophs and autotrophs to the N$_2$O production. This analysis shows that N$_2$O is mainly produced through the AOB pathway but it is to a significant extent consumed by heterotrophic denitrification. Overall, the total N$_2$O production by AOB is 290 % of the net
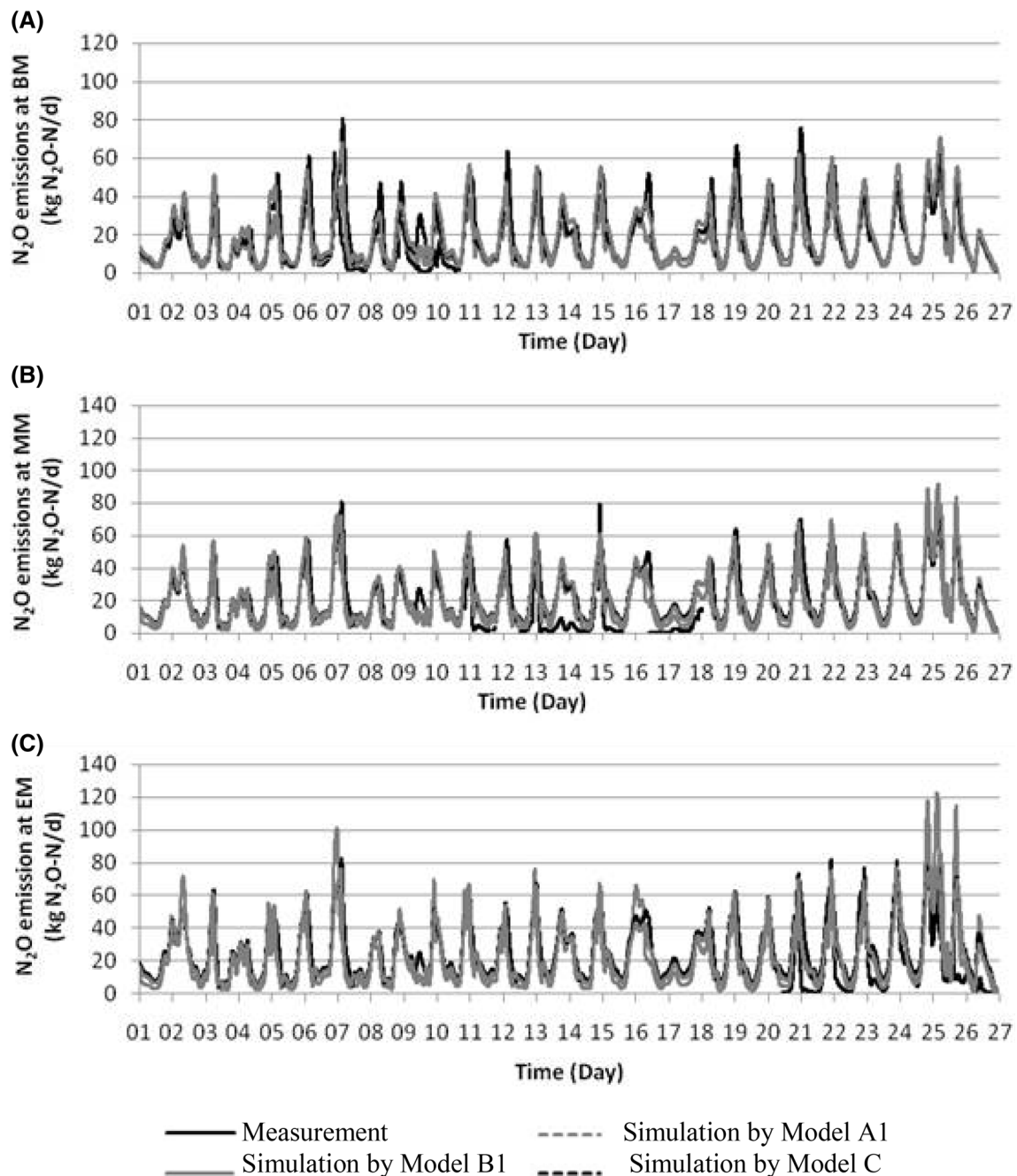
**Fig. 6** Comparison of simulated and measured $N_2O$ emissions at the beginning (BM) (**a**), the middle (MM) (**b**) and the end section (EM) (**c**) of the summer aeration package at the UCT plant

production while the heterotrophs contribute by $-190\%$ [6], i.e. for every three molecules of $N_2O$ produced by AOB, two are removed by heterotrophs. These results thus clearly confirm the need of a good prediction for AOB-related $N_2O$ production as well as heterotrophic denitrification by $N_2O$. Another important factor in such system when using AOB denitrifying models is that a good NOB growth model is needed to be able to predict nitrite concentrations which impact $N_2O$ production by AOB [22].

This means that the ratio between AOB and NOB maximal growth rates as well as respective values of affinity constants for oxygen should be appropriately calibrated, which would determine the quality of nitrite prediction during daily peak loads and concomitantly the $N_2O$ productions.

Table 4 summarises the models capabilities for the different case-studies. The simulations indicate that all five models can correctly describe the ammonium, nitrite and nitrate measurements. Concerning $N_2O$ emissions all the

**Table 4** Comparison of the models' capabilities after calibration on the different case-studies

| Models | System | | | |
|---|---|---|---|---|
| | SBR1 | OD | SBR2 | AS-UCT |
| Model A | ± | − | − | |
| Model A1 | + | | | + |
| Model B | + | + | + | |
| Model B1 | + | | | + |
| Model C | − | + | + | + |

experimental data can be correctly described by at least one (or several) models. Satisfying predictions were observed with AOB denitrification models for SBR1 in which the nitrite concentration varied significantly, the best results being obtained with models considering FNA instead of total nitrite as the substrate for AOB denitrification (A1, B, B1). On the contrary it was not possible to predict the data with Model C based on incomplete oxidation of hydroxylamine, as the effect of nitrite (or FNA) was not considered in this model. In addition, NO emissions were also predicted more accurately with the AOB denitrification model (see data from SBR1). For the OD and SBR2 systems in which nitrite did not accumulate, the simulations with model B and C were in agreement with the observations whereas the other model based on AOB denitrification (Model A) failed. Finally, for the UCT system, Models A1, B1 and C could not be discriminated given by the data set collected, all performed adequately.

Overall it can be stated that the model based on the hydroxylamine pathway was able to match most of the data except for the system with important transient nitrite accumulation (SBR1). On the other hand, the models based on AOB denitrification were able to fit most of the data, either those using hydroxylamine as a state variable (A, A1) or those which do not (B, B1). Concerning the effect of DO, for the systems well described by the AOB denitrification concept (SBR1, UCT) the functions used to reduce $N_2O$ emissions when oxygen increases slightly improved the predictions (Model B1, A). The use of the Haldane expression in Model B1 (instead of the inhibition term only in Model A) allows to predict more accurately the data obtained in the UCT process which exhibited large variation of DO from 0.4 to more than 6 mg $O_2$/L. However, it must be stated that Models A1 and C were also able to reasonably fit the same data without this oxygen inhibition term. In the SBR working with high nitrite accumulation (SBR1) the DO was not very influential in the range presented here (from 2 to 6 mg$O_2$/L) and for this reason the models which do not consider DO inhibition (A1, B) were able to describe the observations as well as the Model B1

with Haldane expression (with relatively high inhibition constant). Hence, it is not possible here to conclude definitively on the benefit of considering inhibition by oxygen. Moreover, higher $N_2O$ production (measured in the liquid phase) was observed in the OD process in zones with higher dissolved oxygen, which further supports a positive correlation between $N_2O$ emissions and DO in this system. It is important to note that the influence of oxygen differs among the predominant pathways. The model based on the hydroxylamine pathway describes the observations of the oxidation ditch better because $N_2O$ is positively related to oxygen in that pathway, assumed to be predominant in that system (due to the low nitrite concentration). On the other hand, a slight decrease of $N_2O$ emission with increased DO was observed in SBR1. In that systems the predominant pathway is likely to be the ND pathway which is logically reduced by increasing the oxygen concentration. In conclusion, the available data were not sufficiently discriminant for this question regarding the oxygen effect but it is suggested to evaluate in the future a multiple pathway model with different effect of oxygen on the emission depending on the pathway.

## Comparison of parameter sets

It should be noted that these properties of the five different models were obtained after significant calibration efforts, and thus the key parameter variations as well as their physical significance are also highly relevant when discussing the validity of the models. All the parameter sets of the models are given in the supplementary information (Tables S3, S4, S5, S6). Table 5 presents the range of variation of the set of AOB parameter values obtained after calibration of each model to the different case studies. Some of the parameters exhibit a large variation among the case studies (more than 100 %), which means that they need to be significantly modified from one case to another. The reduction factor $\eta_{AOB}$, the half saturation constant for nitrite or FNA (for models A, A1, B, B1), and the half saturation constant for NO (Model C) are at the same time highly variable among the case studies and very influential on $N_2O$ and NO emission results. For instance for different systems which were correctly predicted, the reduction factor varied from 0.08 to 0.63 for Model B and similar variations were observed for the other models based on denitrification pathway. For Model C, based on the other concept, the calibration needed important adjustment of the affinity constant ($K_{NO}$ from $8.4 \times 10^{-3}$ to $7 \times 10^{-2}$ mg/L, $K_{NH2OH}$ from 0.1 to 2.4 mg/L). None of the models was able to predict all measured $N_2O$ data sets without significant parameter adjustment. On the one hand, this agrees with the finding of Ni et al. [14] through model evaluation with batch data that it is difficult to predict data obtained

**Table 5** Range of variation of parameters for the different case-studies

| Model A | | Model A1 | | Model B | | Model B1 | | Model C | |
|---|---|---|---|---|---|---|---|---|---|
| $K_{NO2,AOB}$ | 173 % | $K_{HNO2,AOB}$ | 141 % | $K_{HNO2,AOB}$ | 168 % | $K_{HNO2,AOB}$ | 141 % | $K_{NO,AOB}$ | 139 % |
| $\eta_{AOB}$ | 86 % | $K_{NH3,AOB}$ | 141 % | $\eta_{AOB}$ | 71 % | $K_{NH3,AOB,den}$ | 140 % | $K_{O2,AOB,2}$ | 109 % |
| $K_{NH4,AOB}$ | 46 % | $K_{NH2OH,AOB}$ | 140 % | $K_{NH3,AOB}$ | 44 % | $K_{NH3,AOB}$ | 138 % | $K_{NH4,AOB}$ | 81 % |
| $K_{NO,AOB}$ | 37 % | $K_{I,NH3,AOB}$ | 133 % | $K_{O2,AOB}$ | 38 % | $K_{NO,AOB}$ | 131 % | $K_{NH2OH,AOB}$ | 63 % |
| $\mu_{AOB,AMO}$ | 35 % | $K_{O2,AOB,1}$ | 114 % | $K_{NO,AOB}$ | 37 % | $K_{O2,AOB,den}$ | 123 % | $K_{O2,AOB,1}$ | 60 % |
| $\mu_{AOB,HAO}$ | 28 % | $\eta_{AOB}$ | 61 % | $\mu_{AOB}$ | 19 % | $\eta_{AOB}$ | 71 % | $\eta_{AOB}$ | 51 % |
| $K_{I,O2,AOB}$ | 23 % | $K_{NO,AOB}$ | 61 % | $i_{N,AOB}$ | – | $K_{I,O2,AOB}$ | 61 % | $\mu_{AOB,HAO,1}$ | 40 % |
| $K_{O2,AOB,2}$ | 12 % | $\mu_{AOB,HAO}$ | 45 % | $Y_{AOB}$ | – | $K_{O2,AOB}$ | 33 % | $\mu_{AOB,HAO,2}$ | 40 % |
| $K_{O2,AOB,1}$ | – | $\mu_{AOB,AMO}$ | 24 % | $Y_{AOB,den}$ | – | $Y_{AOB}$ | 13 % | $\mu_{AOB,AMO}$ | 29 % |
| $i_{N,AOB}$ | – | $K_{O2,AOB,2}$ | 28 % | | | $\mu_{AOB}$ | 6 % | $Y_{AOB}$ | 10 % |
| $K_{NH2OH,AOB}$ | – | $Y_{AOB}$ | 13 % | | | $i_{N,AOB}$ | – | $Y_{AOB,den}$ | 10 % |
| $Y_{AOB}$ | – | $Y_{AOB,den}$ | 13 % | | | $Y_{AOB,den}$ | – | $i_{N,AOB}$ | – |
| $Y_{AOB,den}$ | – | $i_{N,AOB}$ | – | | | | | | |

under various operating conditions with models based on a single pathway. On the other hand, this comparison using long-term data provides new information which allows evaluating the range of application of each model.

Concerning the models based on the AOB denitrification pathway (e.g. A1, B1), the large variation of some parameters among the case-studies seemed to be related to the range of nitrite (or FNA) concentrations observed in each system. This can be illustrated by two case studies with important difference in the nitrite concentration range: the SBR1 and the UCT process. In Fig. 7, the influence of the FNA concentration on the simulated NO production rate is represented for these two models (A1, B1) calibrated for the SBR1 and UCT systems, respectively. It should be pointed out that the $N_2O$ production rate is correlated to the NO production rate as NO is the precursor for $N_2O$ in these



**Fig. 7** Relation between NO production rate and FNA concentration with AOB denitrification models (A1, B1) calibrated on different data (example of UCT and SBR1)

models. In the system with low nitrite concentration (UCT), a high value for $\eta_{AOB}$ (0.3–0.5) and a low value for $K_{HNO2,AOB}$ ($10^{-5}$–$10^{-6}$) are obtained to fit the observed NO and $N_2O$ emission data. In such situation, the accuracy and the physical significance of the parameters must be evaluated with caution. Indeed, the factor $\eta_{AOB}$ defined originally as a reduction factor for (anoxic) AOB denitrification becomes very high and the affinity constant for FNA is poorly identifiable. With these parameter values the $N_2O$ production rate is little affected by the nitrite concentration, except for very low concentrations. In comparison, a lower value for $\eta_{AOB}$ (0.1–0.2) and a higher value for $K_{HNO2,AOB}$ ($2 \times 10^{-3}$) were obtained during the calibration of the models on the SBR1 process. With those parameters a variation of the FNA concentration influences the NO and $N_2O$ production rates significantly.

These large variations of parameters from one system to another could be explained by different reasons: microorganisms history and adaptation, defaults in the structure of the models, undescribed local heterogeneities in reactor. The nitrifying bacteria are indeed able to acclimatise in different ways to the environmental situations, substrate or inhibitors levels. Adaptation of enzymatic activity (NirK for instance) possibly occurs in these systems. Considering this physiological adaptation the problem with actual model structures is that model constants should actually be treated as model variables. The observed differences could be also due to different nitrifying communities. Based on the observation of Terada et al. [23], the *Nitrosospira* could be adapted to continuously fed process (UCT, OD) and *Nitrosomonas* in SBRs for instance. This would mean that the calibration realised at low nitrite concentrations (and low loaded process) is not valuable in a system with high nitrite accumulation in high loaded process (and vice versa).
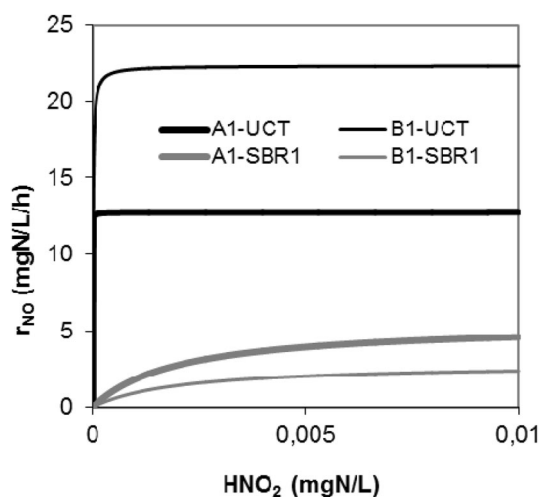
Alternatively, it could be that the second pathway-based on hydroxylamine incomplete oxidation is also present in parallel to the denitrification pathway. In that case a model that considers both pathways would have potential as it could possibly describe a larger range of experimental conditions with a single parameter set, a desirable property as it reduces the calibration effort [16]. In case further experiments confirm that adaptation actually occurs, calibration will remain to be required.

Finally, a limit of the modelling exercise with full-scale processes is to not consider the non-ideality nature of mixing and diffusion within the mixed liquor such that measurements of ammonia and nitrite at the macro-scale (in the bulk) solution may not be representative of what the bacteria are actually experiencing at the micro-scale. In case of significant heterogeneities the values of parameters lump biochemical and physical phenomenon. This could be also an explanation for the differences in parameter values observed for a perfectly mixed reactor lab-scale reactor (SBR1) and full-scale reactors (OD, UCT, SBR2).

## Relation between N$_2$O pathways and nitrite (or FNA) concentration

From the model comparison it can be concluded that the AOB denitrification models are able to describe N$_2$O emissions from the SBR process with high nitrite variation whereas the NH$_2$OH/NO model (C) is not able to predict this system. For all the other systems with low nitrite concentration, the model based on the hydroxylamine pathway (C) fits well with the observations, as well as the models based on AOB denitrification after critical adaptation of some parameters. This supports the assumption that regulation of the N$_2$O production pathway could be influenced by the free nitrous acid (FNA) concentration. For example, the maximal nitrite concentration in the OD and SBR2 are, respectively, around 0.67 and 1.53 mg N/L, with pH close to 7.1. This corresponds to 0.16 and 0.32 µg N-FNA/L, respectively at 15 °C. It was also observed that in SBR1 the production of N$_2$O decreases very significantly when the FNA concentration was lower than 0.5 µgN-FNA/L. It could be speculated that this value could be the limit below which the AOB denitrification processes become less significant compared to the hydroxylamine oxidation pathway. On the other hand, in the UCT system the highest observed nitrite concentration was only 0.11 mgN/L and the Models A1, B1 and C were able to describe the observed trends. Obviously as discussed previously for full-scale processes the measurements of FNA in bulk solution may be not representative of what the bacteria actually experience transiently in some local zone where nitrite can accumulate punctually. In contrast, the pilot SBR can be considered as a perfectly mixed system. In this reactor, the analysis of the variation of NO:N$_2$O ratio and N$_2$O emissions also supported the idea that nitrite stimulated the AOB denitrification pathway [18, 24].

Indeed, it seems logical that the pathway-based on nitrite denitrification was favoured when nitrite accumulates. As it is related to a competition for electrons between nitrite and oxygen as electron acceptors, this competition process should be more intensive at a high FNA:DO ratio, or in case of alternating anoxic–aerobic phases. Considering the model structures, models based on AOB denitrification correlate the N$_2$O production rate to nitrite, whereas the NH$_2$OH oxidation models correlate the N$_2$O production to the ammonium uptake rate. This should be considered for future applications when selecting one of these models. In addition, these observations may help the future development of a generic model involving both the AOB denitrification and the NH$_2$OH pathways. Finally, it is good to mention that these results are in accordance with the results of the quantification of the origin of N$_2$O during nitrification based on isotope signatures [25–27]. Wunderlin et al. [27] demonstrated that the nitrite reduction pathway was the major mechanism responsible for N$_2$O production during batch feeding with ammonium and nitrite. In contrast, the hydroxylamine oxidation pathway became the major process as soon as hydroxylamine accumulated or was injected. The contribution of nitrite reduction pathway was also observed to increase with the nitrite accumulation over time [25, 27]. A recent study also indicated that very high nitrite concentration can also inhibit the AOB denitrification pathway [28]. Given the role of nitrite and FNA in determining N$_2$O emissions and pathways in some of the systems, the ability of AOB/NOB growth models to predict nitrite buildup would also be a key point for future modelling exercises.

## Conclusions

The continuous long-term data sets collected from four different biological processes and the calibration results obtained for different model structures compiled in this paper lead to the following conclusions.

- All the collected N$_2$O data can be described by at least one (or several) model(s) tested in this study and the results allow evaluating the most appropriate N$_2$O model for each system and operational condition.
- Concerning the two different model concepts for N$_2$O production by AOB: the hydroxylamine pathway model can describe most of the data except for those obtained from a system with transient high accumulation of nitrite; the models based on AOB denitrification can fit

most of the data except when inappropriate kinetic was considered for DO inhibition.

- None of the models were able to describe the data with similar parameter sets obtained in systems with high and low nitrite concentrations. A significant calibration effort is necessary for each system, in some cases leading to extreme and controversial values for parameters. Variability of the parameters can be related to physiological adaptation of micro-organisms, a microbial population switch, regulation between multiple AOB pathways or difficulties related to undescribed local concentration heterogeneities.

- The regulation between the $N_2O$ production pathways is likely correlated with (variation of) the nitrite concentration in the system. Future efforts will be deployed to evaluate a more generic model in which the enzymatic regulation and/or the interaction between both AOB pathways are described, and it will be necessary to evaluate whether such approach could extend the model validity and reduce calibration effort.

# References

1. Ahn JH, Kim S, Park H et al (2010) $N_2O$ emissions from activated sludge processes, 2008–2009: results of a national monitoring survey in the US. Environ Sci Technol 44:4505–4511. doi:10.1021/es903845y

2. Kampschreur MJ, Temmink H, Kleerebezem R, Jetten MS, van Loosdrecht MC (2009) Nitrous oxide emission during wastewater treatment. Water Res 43:4093–4103. doi:10.1016/j.watres.2009.03.001

3. Daelman MRJ, van Voorthuizen EM, van Dongen UGJM, et al. (2013) Full-scale evaluation of process conditions leading to the emission of nitrous oxide from municipal wastewater treatment plants. In: Proceedings of WEF/IWA nutrient removal and recovery 2013: trends in resource recovery and use. Vancouver, British Columbia, Canada, July 28–31

4. Guo L, Lamaire-Chad C, Bellandi G, Daelman M, Amerlinck Y, Maere T, Nous J, Flameling T, Weijers S, van Loosdrecht MCM, Volcke EIP, Nopens I, Vanrolleghem PA (2013a) High-Frequency Field Measurement of Nitrous oxide ($N_2O$) Gas emissions and influencing factors at WWTPs under dry and wet weather conditions. In: Proceedings of WEF/IWA nutrient removal and recovery 2013: trends in resource recovery and use. Vancouver, British Columbia, Canada, July 28–31

5. Wunderlin P, Mohn J, Joss A, Emmenegger L, Siegrist H (2012) Mechanisms of $N_2O$ production in biological wastewater treatment under nitrifying and denitrifying conditions. Water Res 46:1027–1037

6. Guo L, Vanrolleghem PA (2013) Calibration and validation of an activated sludge model for greenhouse gases no. 1 (ASMG1): prediction of temperature-dependent $N_2O$ emission dynamics. Bioprocess Biosyst Eng. doi:10.1007/s00449-013-0978-3

7. Castro-Barros CM, Daelman MRJ, Mampaey KE, van Loosdrecht MC, Volcke EI (2015) Effect of aeration regime on $N_2O$ emission from partial nitritation-anammox in a full-scale granular sludge reactor. Water Res 68:793–803. doi:10.1016/j.watres.2014.10.056

8. Hiatt WC, Grady CPL (2008) An updated process model for carbon oxidation, nitrification, and denitrification. Water Environ Res 80:2145–2156. doi:10.2175/106143008X304776

9. Pan Y, Ni B-J, Yuan Z (2013) Modeling electron competition among nitrogen oxides reduction and $N_2O$ accumulation in denitrification. Environ Sci Technol 47:11083–11091. doi:10.1021/es402348n

10. Chandran K, Stein LY, Klotz MG, van Loosdrecht MCM (2011) Nitrous oxide production by lithotrophic ammonia-oxidizing bacteria and implications for engineered nitrogen-removal systems. Biochem Soc Trans 39:1832–1837. doi:10.1042/BST20110717

11. Stein LY (2011) Surveying $N_2O$-producing pathways in bacteria. Methods Enzymol 486:131–152. doi:10.1016/B978-0-12-381294-0.00006-7

12. Mampaey KE, Beuckels B, Kampschreur MJ, Kleerebezem R, van Loosdrecht MC, Volcke EI (2013) Modelling nitrous and nitric oxide emissions by autotrophic ammonia-oxidizing bacteria. Environ Technol 34:1555–1566

13. Ni B-J, Ruscalleda M, Pellicer-Nàcher C, Smets BF (2011) Modeling nitrous oxide production during biological nitrogen removal via nitrification and denitrification: extensions to the general ASM models. Environ Sci Technol 45:7768–7776. doi:10.1021/es201489n

14. Ni B-J, Yuan Z, Chandran K, Vanrolleghem PA, Murthy S (2013) Evaluating four mathematical models for nitrous oxide production by autotrophic ammonia-oxidizing bacteria. Biotechnol Bioeng 110:153–163. doi:10.1002/bit.24620

15. Ni B-J, Ye L, Law Y, Byers C, Yuan Z (2013) Mathematical modeling of nitrous oxide ($N_2O$) emissions from full-scale wastewater treatment plants. Environ Sci Technol 47:7795–7803. doi:10.1021/es4005398

16. Ni B-J, Peng L, Law Y, Guo J, Yuan Z (2014) Modeling of nitrous oxide production by autotrophic ammonia-oxidizing bacteria with multiple production pathways. Environ Sci Technol 48:3916–3924. doi:10.1021/es405592h

17. Guo L, Vanrolleghem PA (2014) Full-scale simulation of $N_2O$ emissions with ASMG2d and elucidation of its different production and emission sources in nitrogen (N) and phosphorus (P) removed systems **(Under review)**

18. Pocquet M, Queinnec I, Spérandio M (2013) Adaptation and identification of models for nitrous oxide ($N_2O$) production by autotrophic nitrite reduction. In: Proceedings 11th IWA conference on instrumentation, control and automation (ICA2013). Narbonne, France, September 18–20

19. Ye L, Ni B-J, Law Y, Byers C, Yuan Z (2014) A novel methodology to quantify nitrous oxide emissions from full-scale wastewater treatment systems with surface aerators. Water Res 48:257–268. doi:10.1016/j.watres.2013.09.037

20. Reichert P (1998) User manual, computer program for the identification and simulation of aquatic systems

21. Vanhooren H, Meirlaen J, Amerlinck Y, Claeys F, Vangheluwe H, Vanrolleghem PA (2003) WEST: modelling biological wastewater treatment. http://www.iwaponline.com/jh/005/jh0050027.htm. Accessed 29 Nov 2014

22. Houweling D, Wunderlin P, Dold P, Bye C, Joss A, Siegrist H (2011) N$_2$O emissions: modeling the effect of process configuration and diurnal loading patterns. Water Environ Res 83:2131–2139

23. Terada A, Sugawara S, Yamamoto T, Zhou S, Koba K, Hosomi M (2013) Physiological characteristics of predominant ammonia-oxidizing bacteria enriched from bioreactors with different influent supply regimes. Biochem Eng J 79:153–161. doi:10.1016/j.bej.2013.07.012

24. Pocquet M, Wu Z, Queinnec I, Spérandio M (2016) A two pathway model for N$_2$O emissions by ammonium oxidizing bacteria supported by the NO/N2O variation. Water Res 88:948–959

25. Rathnayake RMLD, Song Y, Tumendelger A, Oshiki M, Ishii S, Satoh H, Toyoda S, Yoshida N, Okabe S (2013) Source identification of nitrous oxide on autotrophic partial nitrification in a granular sludge reactor. Water Res 47:7078–7086. doi:10.1016/j.watres.2013.07.055

26. Toyoda S, Suzuki Y, Hattori S, Yamada K, Fujii A, Yoshida N, Kouno R, Murayama K, Shiomi H (2011) Isotopomer analysis of production and consumption mechanisms of N$_2$O and CH$_4$ in an advanced wastewater treatment system. Environ Sci Technol 45:917–922. doi:10.1021/es102985u

27. Wunderlin P, Lehmann MF, Siegrist H, Tuzson B, Joss A, Emmenegger L, Mohn J (2013) Isotope signatures of N$_2$O in a mixed microbial population system: constraints on N$_2$O producing pathways in wastewater treatment. Environ Sci Technol 47:1339–1348. doi:10.1021/es303174x

28. Law Y, Lant P, Yuan Z (2013) The confounding effect of nitrite on N$_2$O production by an enriched ammonia-oxidizing culture. Environ Sci Technol 47:7186–7194. doi:10.1021/es4009689